BUCKLING INSTABILITY OF CARBON NANOSCROLLS AND ITS POTENTIAL APPLICATIONS

Teng Li[*a)] , Zhao Zhang[*] & Yinjun Huang[*]
[*]*Department of Mechanics Engineering, University of Maryland, College Park, MD, USA 20742*

Summary Formed by rolling up a monolayer graphene into a spiral structure, a carbon nanoscroll (CNS) is topologically open and has two free edges along axial direction, distinct from a multiwalled carbon nanotube (MWCNT). We show that, the unique structure of a CNS dictates distinct features of its buckling instability under axial compression, twist and bending from those of a MWCNT. The understanding of reversible buckling instability of CNSs could potentially enable novel nano-device concepts.

INTRODUCTION

Surging interests in graphene in past several years[1] open pathways to investigating a new member in this family — carbon nanoscrolls (CNSs)[2,3]. A CNS is formed by rolling up a monolayer graphene into a spiral multilayer nanostructure (Fig. 1), thus is topologically open. By contrast, a CNT is topologically closed. The unique structure of CNSs has inspired an array of novel nano-device applications, such as hydrogen storage medium[4], ultra-fast nano-oscillators[3,5] and nano-actuators[6]. Meanwhile, the topologically open structure of CNSs suggests the proneness of CNSs to buckling instability under mechanical loads. The success of CNS-based device applications crucially hinges upon systematic understanding of the buckling instability of CNSs, a topic that remains largely unexplored.

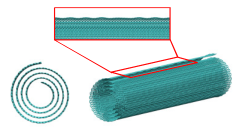

FIG. 1. The perspective and cross-section views of a 4-layer CNS. Note the intrinsic wrinkles along the free edge of the CNS.

Buckling instability of CNTs has been extensively studied in recent years[8]. However, the fundamental difference in the topology of a CNS and a MWCNT dictates their dissimilar deformation behaviors, and thus renders distinct characteristics of the buckling instability of the CNS from that of the MWCNT. In this paper, we report the first systematic study of the buckling instability of CNSs under axial compression, torsion, and bending, using molecular mechanics simulations, aiming to decipher the difference in critical buckling conditions of CNSs and MWCNTs.

BUCKLING INSTABILITY OF CNSs UNDER COMPRESSION, TORSION AND BENDING

The CNSs in the simulations have a length of 20 nm and diameters from 2 nm to 6 nm depending on the number of layers, with its spiral ends being armchair. As a comparison with an *n*-layer CNS, an *n*-layer MWCNT with the same length is also modeled. The REBO potential[9] and 12-6 Lennard-Jones potential[10] are adopted to describe the C-C covalent interaction and vdW force, respectively. During the simulation, loading is applied onto the structures incrementally and the potential energy is minimized between two loading increments.

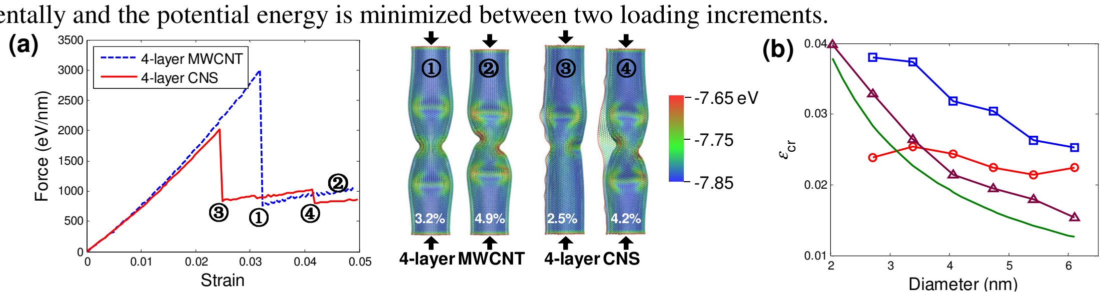

FIG. 2 (a) Axial force as a function of axial compressive strain for a 4-layer CNS (solid line) and a 4-layer MWCNT (dashed line), respectively. Insets 1 and 2 show the deformed shapes of the 4-layer MWCNT at a strain of 3.2% (right after onset of buckling) and a postbuckling strain of 4.9%, respectively. Insets 3 and 4 show the deformed shapes of the 4-layer CNS at a strain of 2.5% (right after onset of buckling) and a postbuckling strain of 4.2%, respectively. (b) Critical buckling onset strains ε_{cr} of a MWCNT, a CNS and a SWCNT as a function of their diameter, respectively.

Figure 2a plots the axial force vs. applied strain curves of a 4-layer CNS and a 4-layer MWCNT under axial compression, respectively. The sharp drop of the axial force in each curve indicates the onset of buckling. While the 4-layer MWCNT buckles at a critical axial compressive strain of $\varepsilon_{cr} = 3.2\%$, the 4-layer CNS buckles at a much smaller $\varepsilon_{cr} = 2.5\%$. The snapshots of the 4-layer MWCNT and the 4-layer CNS right after buckling onset are shown in insets 1 and 3 in Fig. 2a, respectively. Figure 2b plots ε_{cr} of CNS and MWCNT as a function of their diameter, respectively. ε_{cr} of a MWCNT decreases significantly as its diameter increases. Interestingly by contrast, ε_{cr} of a CNS remains approximately a constant, nearly independent on its diameter. For a CNS, the wrinkles along its free edges (especially the outer free edge that is less constrained) are highly vulnerable to further buckling under compression (e.g., inset 3 in Fig. 2a), which can further propagate along the spiral basal graphene through C-C covalent bonds, resulting in the overall buckling of the CNS. In other words, ε_{cr} of a CNS under compression is largely dictated by the intrinsic fluctuations along its free edges, thus is nearly independent on its diameter.

Figure 3a plots the resultant torque as functions of twist angle per unit length for a 4-layer CNS and a 4-layer MWCNT, respectively. The distinction between the CNS and the MWCNT under torsion is threefold. First, the CNS has much

a) Corresponding author. Email: LiT@umd.edu

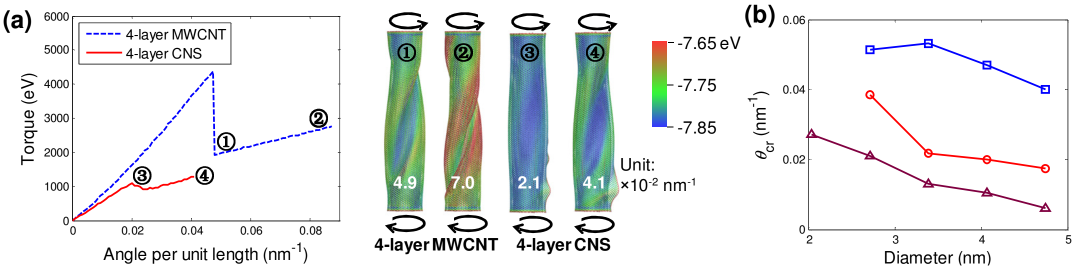

FIG. 3 (a) Resultant torque as a function of twist angle per unit length for a 4-layer CNS (solid line) and a 4-layer MWCNT (dashed line), respectively. Insets 1 and 2 show the deformed shapes of the 4-layer MWCNT at a twist angle of 0.049 nm^{-1} and a postbuckling twist angle of 0.07 nm^{-1}, respectively. Insets 3 and 4 show the deformed shapes of the 4-layer CNS at a twist angle of 0.021 nm^{-1} and a postbuckling twist angle of 0.041 nm^{-1}, respectively. (b) Critical buckling onset twist angle θ_{cr} of a MWCNT, a CNS and a SWCNT as a function of their diameter, respectively.

smaller torsion rigidity than the MWCNT before buckling onset, indicated by initial slope of the two curves. Second, the critical buckling onset twist angle θ_{cr} for the CNS is much smaller than that of the MWCNT. For example, θ_{cr} = 0.047 nm^{-1}for the 4-layer MWCNT, and 0.020 nm^{-1} for the 4-layer CNS. Third, the drop in resultant torque for the 4-layer CNS at the onset of buckling is much smaller and less sharp than that for the 4-layer MWCNT. These distinctions in the deformation behavior between CNS and MWCNT can be largely attributed to the open topology of CNS. Figure 3b plots θ_{cr} of a MWCNT, a CNS and a SWCNT as a function of their diameter, respectively. Though in general θ_{cr} decreases as the diameter of the MWCNT, CNS or SWCNT increases, θ_{cr} of a CNS is much lower than that of a MWCNT of the same diameter and only slightly higher than that of a SWCNT of the same diameter.

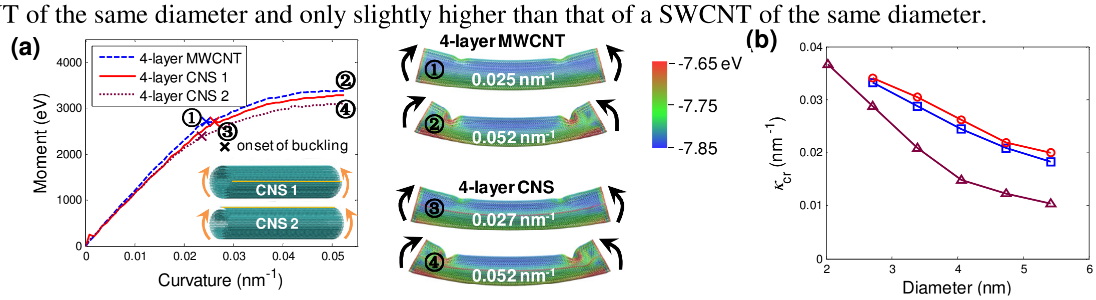

FIG. 4 (a) Resultant bending moment as a function of curvature for a 4-layer MWCNT (dashed line) and two 4-layer CNSs (solid and dotted lines), respectively. Insets 1 and 2 show the deformed shapes of the 4-layer MWCNT at a curvature of 0.025 nm^{-1} and 0.052 nm^{-1}, respectively. Insets 3 and 4 show the deformed shapes of the 4-layer CNS at a curvature of 0.027 nm^{-1} and 0.052 nm^{-1}, respectively. (b) Critical buckling onset curvature κ_{cr} of a MWCNT, a CNS and a SWCNT as a function of their diameter, respectively.

Figure 4a plots the resultant bending moment as a function of curvature for a 4-layer MWCNT and two 4-layer CNS (with different loading direction), respectively. The bending rigidity of the 4-layer CNS is slightly smaller than that of the 4-layer MWCNT. At the onset of buckling, two kinks set in on the compressive side of the CNS (or the MWCNT) and there is no significant drop in the resultant bending moment. The critical curvature for buckling, κ_{cr}, is then determined by the applied curvature at the onset of kink formation in the CNS and MWCNT under bending. κ_{cr} of the 4-layer MWCNT is 0.024 nm^{-1}, and that of the 4-layer CNS are 0.026 nm^{-1} or 0.023 nm^{-1} (in two loading directions, respectively). Further simulations show similar deformation and buckling behaviors of CNSs and MWCNTs with various diameters (2 to 6 layers) (Fig. 4b). The bending rigidity of a CNS increases and its κ_{cr} decreases as its diameter increases, so does that of a MWCNT. κ_{cr} of a CNS is only slightly smaller than that of a MWCNT of the same diameter. Bending buckling of the CNS (or the MWCNT) causes only rather localized kinks, thus the difference in cross-section topology between a CNS and a MWCNT has negligible effect on their bending buckling behavior.

CONCLUSIONS

In summary, we report first systematic study of the buckling instability of CNSs under mechanical loads. The unique open topology of CNSs and the existence of two free edges in CNSs render distinct features of buckling instability from those of MWCNTs. Results from this study could lead to a better understanding of the mechanical reliability of CNS-based electromechanical devices. The distinct buckling features of CNSs could shed light on new device concepts.

References

1 A. K. Geim and A. H. MacDonald, Physics Today **60** (8), 35 (2007); A. K. Geim, Science **324** (5934), 1530 (2009).
2 L. M. Viculis, J. J. Mack, and R. B. Kaner, Science **299** (5611), 1361 (2003); Xu Xie, *et al.* Nano Letters **9** (7), 2565 (2009).
3 X. Shi, *et al.* , Applied Physics Letters **95** (16), 163113 (2009).
4 G. Mpourmpakis, E. Tylianakis, G. E. Froudakis, Nano Letters **7** (7), 1893 (2007); V. R. Coluci, *et al.* Physical Review B **75** (12) (2007).
5 Z. Zhang and T. Li, Nanoscale Research Letters **6** (2011).
6 X. Shi, *et al.* Applied Physics Letters **96** (5), 517 (2010).
7 L. Yang and J. Han, Physical Review Letters **85** (1), 154 (2000).
8 B. I. Yakobson, C. J. Brabec, and J. Bernholc, Phys. Rev. Lett. **76** (14), 2511 (1996); K. M. Liew, *et al.* Phys. Rev. B **69** (11) (2004); G. X. Cao and X. Chen, Physical Review B **73** (15) (2006); X. Huang, *et al.* J. Mech. Phys. Solids **58** (11), 1847 (2010); C. M. Wang, *et al.* Appl. Mech. Rev. **63** (3) (2010).
9 D. W. Brenner, *et al.* Journal of Physics: Condensed Matter **14** (4), 783 (2002).
10 S. J. Stuart, A.. Tutein, and J. A. Harrison, The Journal of Chemical Physics **112** (14), 6472 (2000).